

Dual-Energy CT-Derived Iodine Content and Spectral Attenuation Analysis of Metastatic Versus Nonmetastatic Lymph Nodes in Squamous Cell Carcinoma of the Oropharynx

Alexandra M. Foust, Rukya M. Ali, Xuan V. Nguyen, Amit Agrawal, Luciano M. Prevedello, Eric C. Bourekas, and Daniel J. Boulter

The Wexner Medical Center, The Ohio State University, Columbus, OH

Corresponding Author:

Alexandra M. Foust, DO
395 West 12th Avenue, Columbus, OH 43026;
E-mail: alexandra.foust@osumc.edu

Key Words: dual-energy CT, oropharyngeal carcinoma, head and neck

Abbreviations: Dual-energy computed tomography (DECT), ultrasonography (US), computed tomography (CT), magnetic resonance imaging (MRI), region of interest (ROI), receiver operator characteristic (ROC), positron emission tomography (PET)

ABSTRACT

The presence of a single nodal metastasis has significant prognostic and treatment implications for patients with head and neck cancer. This study aims to investigate whether dual-energy computed tomography (DECT)-derived iodine content and spectral attenuation curve analysis can improve detection of nodal metastasis in oropharyngeal carcinoma. Eight patients with newly diagnosed oropharyngeal squamous cell carcinoma and pathologically proven nodal metastatic disease ($n = 13$ metastatic nodes; $n = 16$ nonmetastatic nodes) who underwent contrast-enhanced DECT of the neck were retrospectively evaluated. DECT-derived iodine content (mg/mL) and monoenergetic attenuation values at 40 keV and 100 keV were obtained via circular regions of interest within metastatic and nonmetastatic cervical lymph nodes. Iodine content was significantly lower in metastatic nodes (0.96 ± 0.28 mg/mL) than in nonmetastatic nodes (1.65 ± 0.38 mg/mL; $P = .002$). Iodine spectral attenuation slope was significantly lower in metastatic nodes (1.33 ± 0.49 mg/mL) than in nonmetastatic nodes (1.91 ± 0.64 mg/mL; $P = .015$). A nodal iodine threshold of ≤ 1.3 mg/mL showed a sensitivity of 84.6% and a specificity of 75.0%, with an area under the curve of 0.839, $P < .0001$. At a threshold value of ≤ 1.95 for nodal spectral attenuation slope, an optimized specificity of 92.3% and specificity of 50.0% was achieved, with an area under the curve of 0.68 ($P = .049$). DECT-derived quantitative iodine data and spectral attenuation curves may improve the diagnostic accuracy of computed tomography for nodal metastasis in patients with squamous cell carcinoma of the oropharynx.

INTRODUCTION

Despite growing understanding and continued advances in treatment, both the incidence and mortality rates of head and neck cancer have not significantly changed in the past decade, with $\sim 63,000$ new cases occurring in 2017 and an overall 5-year survival rate of 60%–65%. Squamous cell carcinoma accounts for $>90\%$ of these cases, with the majority of cases occurring in the oral cavity/pharynx ($\sim 79\%$) (1, 2). Imaging plays an important role in the staging of head and neck cancers to define both the extent of invasion of the primary tumor and the presence of locoregional and distant metastases.

Currently, there are many different imaging modalities used in the evaluation and staging of head and neck cancer including ultrasonography (US), computed tomography (CT), magnetic resonance imaging (MRI), and fluorodeoxyglucose-positron emission tomography. Imaging features, which are used to determine the likelihood of metastatic lymph node involvement, rely heavily

on size (size > 10 – 15 mm in the short axis) and shape (circular nodes $>$ ovoid nodes) (3). Visualization of necrosis within a lymph node is also helpful for identifying nodal metastasis when present; however, this can be difficult to detect with current imaging methods. New imaging techniques show promise in integrating morphological and functional changes in lymph nodes to better differentiate metastatic from nonmetastatic nodes.

Dual-energy CT (DECT) provides enhanced diagnostic capabilities by allowing for improved tissue differentiation compared with single-energy CT, which may improve diagnostic accuracy. DECT takes advantage of the change in attenuation of different tissues at different photon energy levels based on the atomic number (Z) of the materials (4). One practical use of this technology is to assess the distribution of iodinated contrast on contrast-enhanced CT scans by creating iodine-only images. Along a similar line, postprocessing can be performed to quantify the amount of

iodine in a given region of interest (ROI). “Virtual monoenergetic” images that simulate a specific desired energy level can also be generated to alter the attenuation and conspicuity of iodinated contrast relative to background tissues compared with standard images. Each of these techniques can be used to increase the visual contrast between normal and abnormal tissues by amplifying the subtle differences in attenuation, which may aid in detection and characterization of tumors and lymph node metastases.

In summary, commonly used imaging features for nodal metastasis in head and neck cancer such as size, shape, and occasional visible necrosis are not always reliable. DECT improves characterization of contrast material distribution within lymph nodes because of energy-dependent differences in the Hounsfield units (HU) of iodine relative to soft tissues. Early studies of DECT show promising results for this technique in the evaluation of head and neck cancer. The purpose of our study was to further evaluate whether DECT iodine content data and spectral HU curve analysis can help differentiate between metastatic and nonmetastatic lymph nodes in patients with newly diagnosed squamous cell carcinoma of the head and neck.

METHODOLOGY

This retrospective study was approved both by the Comprehensive Cancer Center Clinical Scientific Review Committee and the Ohio State Cancer Institutional Review Board, and the requirement for informed consent was waived.

Patients

Following Institutional Review Board approval, 25 patients with newly diagnosed primary squamous cell carcinoma of the head and neck who received a staging DECT of the neck with contrast on a dual-source CT scanner were identified from Spring 2016 to Spring 2017. Of these 25 patients, 8 patients who had pathologically proven primary oropharyngeal carcinomas with at least 1 metastatic lymph node were identified. Up to 2 pathologically proven metastatic lymph nodes per patient were included in the analysis for a total of 13 metastatic lymph nodes. Two pathologically proven nonmetastatic nodes were also identified in each patient for a total of 16 control lymph nodes. Six of the included patients' tumors were human papillomavirus (HPV)-positive and 1 was HPV-negative; the HPV status of the final patient was unknown.

Exclusion criteria included patients with primary oropharyngeal malignancies without pathologic correlation, patients with other primary head and neck carcinomas outside of the oropharynx, patients with other coexisting primary malignancies, patients who received noncontrast staging CT scans or received contrast CT staging scans on a nondual energy scanner, patients with recurrence of previous squamous cell carcinoma of the head and neck, and patients who already received treatment of primary head and neck malignancy. The mean patient age at the time of diagnosis was 54 years, with a standard deviation of 10.4 years. There were 5 male patients (63%) and 3 female patients (37%).

CT and Imaging Postprocessing

IV access was obtained, and patients were positioned in the supine position on the scanner platform of our dual-source

dual-energy CT scanner (second generation, Somatom Definition Flash, Siemens Healthcare, Forchheim, Germany). Fifty mL of iodinated contrast (350 mg/mL) was injected at a rate of 3 mL/s with a 35-second delay to start of scan to allow for imaging acquisition in the venous phase. Dual-energy protocol specifications were as follows: tube A was obtained at 80 kVp with 302 mA of reference; tube B was obtained at 140 kVp and 157 mA of reference. The remaining imaging parameters were the same for both tubes, including a gantry rotation time of 0.28 seconds, a pitch of 0.9, and a collimation section thickness of 0.6 mm. Section thickness was 0.75 mm for both data sets, and no gantry tilt was used.

Metastatic and nonmetastatic lymph nodes of known pathologic status were evaluated by a board-certified neuroradiologist specialized in head and neck radiology. Metastatic lymph nodes were defined according to widely accepted imaging characteristics as meeting at least 2 of the following criteria: nodal size > 10 mm in short axis, visible necrosis, a rounded morphology, and/or loss of the nodal fatty hilum. Control nodes were smaller than 8 mm in size and did not meet any of the aforementioned criteria for metastatic nodes.

Postprocessing was performed on a vendor-specific commercially available dual-energy-equipped workstation (Syngo.via, Siemens, Germany). Circular ROIs were drawn by the neuroradiologist within the primary neoplasm, metastatic lymph nodes, and control lymph nodes, specifically avoiding regions of visible necrosis. Data from these ROIs were recorded, including iodine content (mg/mL), iodine overlay attenuation (HU), virtual non-contrast attenuation (HU), attenuation values at 40 keV (HU), and attenuation at 100 keV (HU).

Iodine Spectral Attenuation Curve

The attenuation of iodine for a given region of interest is represented as a spectral curve representing the change in attenuation values in the ROI over different energy levels (Figure 1). Two representative data points were selected from the spectral curve, one at 40 keV and one at 100 keV, and the slope of a line between these 2 points was then calculated to provide a quantitative data point representation of the spectral attenuation within the ROI (5) (Figure 2).

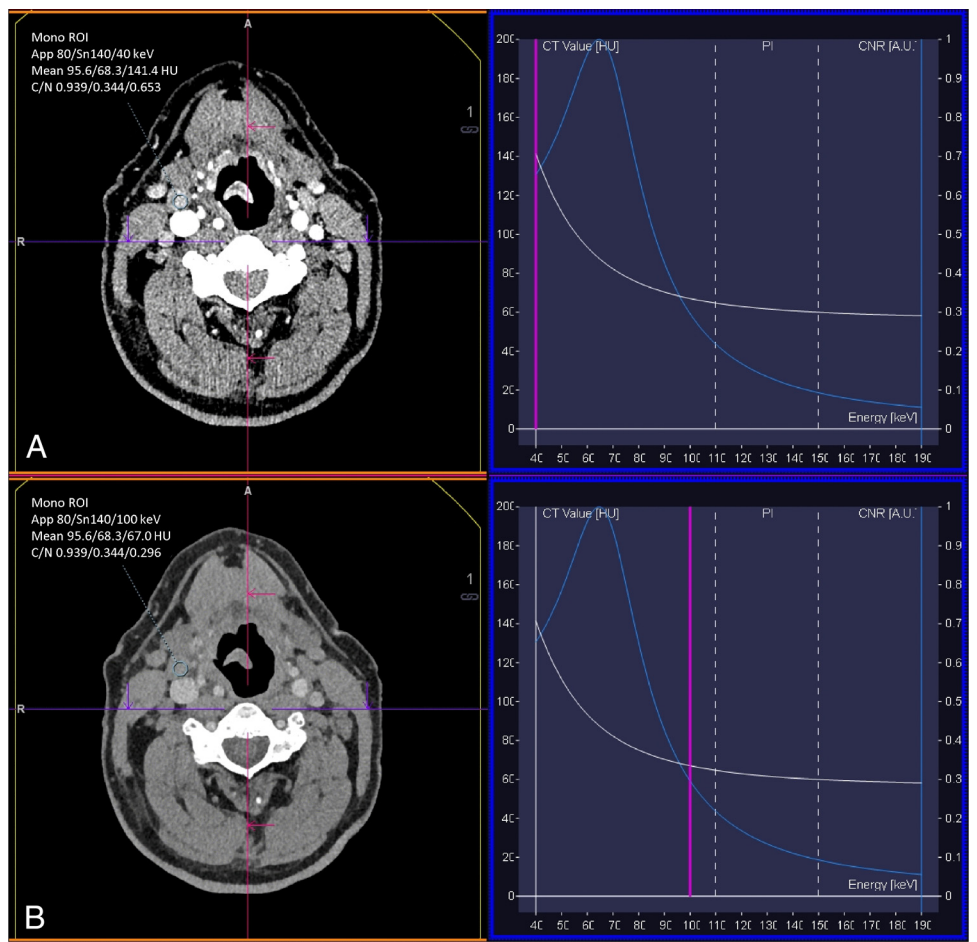
$$\lambda_{\text{HU}} = \frac{(\text{HU}_{40 \text{ keV}} - \text{HU}_{100 \text{ keV}})}{60}$$

This method of spectral attenuation curve analysis has previously been used in the evaluation of both nodal metastases and laryngeal cartilage invasion in patients with laryngeal squamous cell carcinomas (5–7).

Statistical Analysis

Mean values and standard deviations were calculated for metastatic and nonmetastatic nodal iodine content and spectral attenuation slopes and compared via paired *t* tests. Mean values and standard deviations were also calculated for the nodal-to-primary ratios of iodine content and spectral attenuation slopes. XLSTAT statistical software (Paris, France) was used to generate receiver operator characteristic (ROC) curves for nodal iodine content and spectral attenuation slope (8).

Figure 1. Axial virtual monochromatic images at 40 keV (A) and 100 keV (B). Circular regions of interest (ROIs) are drawn within a metastatic lymph node used to measure attenuation at the given energy level. Attenuation values are 141.4 HU and 67.0 HU in the ROIs of 40 keV and 100 keV, respectively.



RESULTS

Iodine Content

The iodine content was significantly lower in metastatic lymph nodes (0.96 ± 0.28 mg/mL) than in nonmetastatic lymph nodes (1.65 ± 0.38 mg/mL; $P = .002$) (Figures 3 and 4). Following a similar trend, the ratio of nodal iodine content to primary malignancy iodine content was also significantly lower for metastatic lymph nodes (0.82 ± 0.28 mg/mL) than for nonmetastatic nodes (1.44 ± 0.55 mg/mL; $P = .009$).

Iodine Spectral Curve Slope

The iodine spectral attenuation curve slope was significantly lower in metastatic lymph nodes (1.33 ± 0.49 mg/mL) than in nonmetastatic nodes (1.91 ± 0.60 mg/mL; $P = .015$) (Figure 5). When the ratio of the nodal spectral slope to the primary malignancy spectral slope was evaluated, the slope was significantly lower for the metastatic-to-primary ratio (1.05 ± 0.50 mg/mL) than for the nonmetastatic-to-primary ratio (1.48 ± 0.62 mg/mL; $P = .023$).

ROC Curves

The ROC curves for nodal iodine content and for nodal spectral attenuation slope are shown in Figure 6. At a threshold nodal iodine content value of ≤ 1.3 mg/mL, sensitivity was 84.6% and specificity was 75.0%. The area under the receiver operating curve for nodal iodine content was 0.839, with a 95% confidence interval of 0.683–0.995 ($P < .0001$). The ROC curve for

the nodal spectral attenuation slope revealed that at a threshold of ≤ 1.95 , there was an optimized sensitivity of 92.3% and a specificity of 50.0%. The area under the receiver operating curve for nodal spectral attenuation slope was 0.680, with the 95% confidence interval of 0.466–0.894 ($P = .049$).

DISCUSSION

To the best of our knowledge, this is the first study to use dual-energy CT to evaluate pathologically proven metastatic nodal disease in patients with primary oropharyngeal squamous cell carcinoma. Given that the presence of a single metastatic lymph node is associated with up to a 50% reduction in the 5-year survival rate in patients with head and neck cancer, improving the diagnostic accuracy of nodal metastatic disease is of utmost importance (9).

In this study, pathologically proven metastatic lymph nodes in patients with oropharyngeal squamous cell carcinoma showed significantly lower iodine content than nonmetastatic lymph nodes. This significant difference persisted when the ratio of metastatic node iodine to primary tumor iodine was compared with the ratio of nonmetastatic node iodine to primary tumor iodine. These findings are in line with a study by Tawfic et al., which evaluated iodine content in cases of various primary squamous cell carcinomas of the head and neck, inflammatory cervical lymph nodes, and normal cervical lymph nodes and found significantly lower iodine content within metastatic lymph nodes compared to inflammatory or nonmetastatic nodes (10). However, Tawfic et al. found an optimal threshold iodine con-

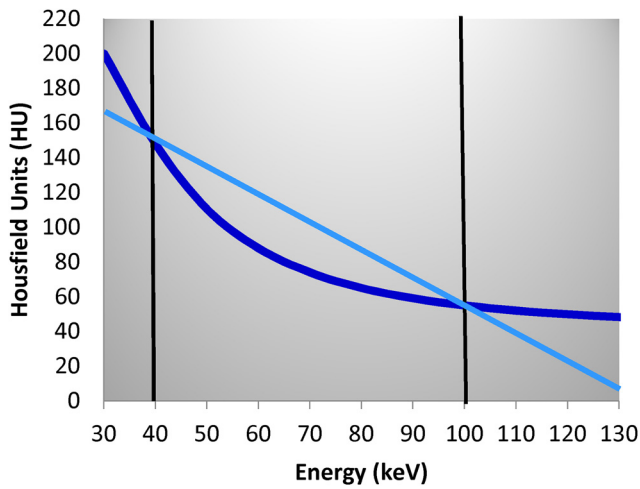


Figure 2. Two representative points (black lines) are selected along the iodine attenuation curve (dark blue line), at 40 keV and 100 keV. A line (light blue) is then drawn between the 2 points from which the slope of the spectral attenuation curve is then calculated.

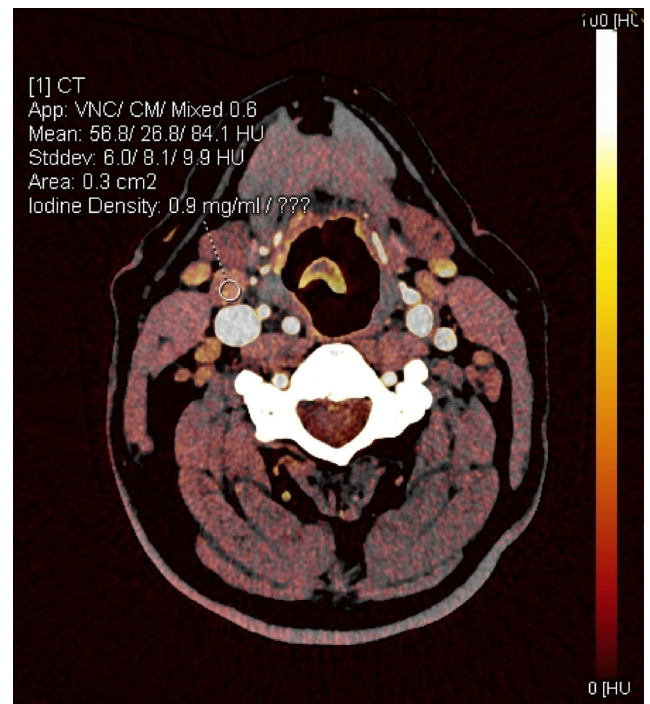


Figure 4. Axial iodine overlay image with ROI drawn in metastatic lymph node. Iodine content within the ROI given in milligram per milliliter.

tent value of ≤ 2.85 mg/mL, whereas our ROC analysis revealed an optimal threshold iodine content value of ≤ 1.3 mg/mL (10). This difference may in part be related to the location of the primary neoplasm, as this study focused specifically on oropharyngeal primaries, whereas Tawfic et al. included various primary head and neck cancers from the oropharynx, hypopharynx, and larynx. Differences between institutions with regard to iodinated contrast volume, concentration, and bolus timing of scan acquisition may also have played a role. At our institution, image acquisition is triggered following a 35-second

delay after administration of 175 mg of iodinated contrast for neck CTs with contrast, whereas Tawfic et al. administered a dose of 400 mg of iodinated contrast and used a 70-second image acquisition delay (10).

While the exact reason for reduced iodine content within metastatic lymph nodes compared with control nodes in

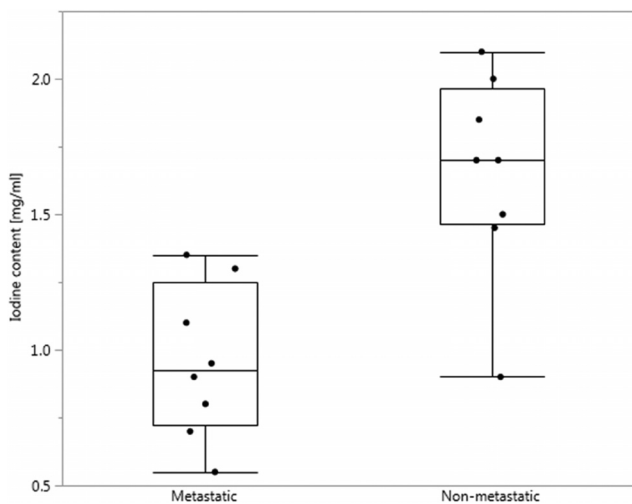


Figure 3. Box-and-whisker plot showing the range of iodine content values within metastatic and nonmetastatic lymph nodes.

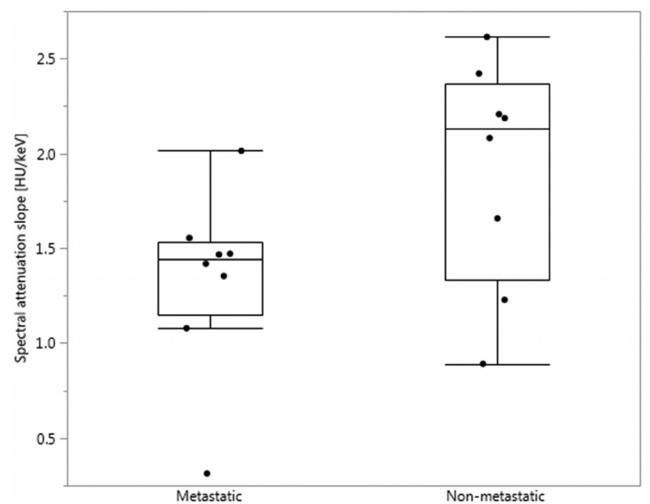
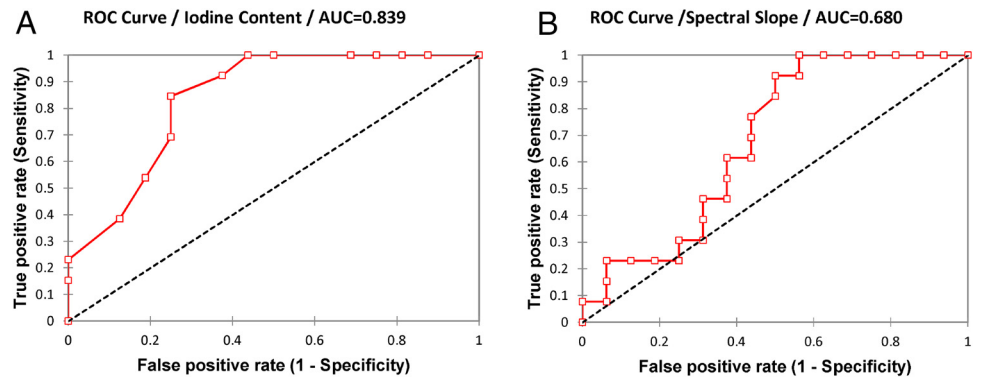


Figure 5. Box-and-whisker plot showing the range of spectral attenuation slopes within metastatic and nonmetastatic lymph nodes.

Figure 6. ROI curves for nodal iodine content (A) and spectral iodine attenuation slope (B). At an iodine content threshold value of ≤ 1.3 mg/mL, there is a sensitivity of 84.6% and a specificity of 75.0%. At a spectral iodine attenuation slope threshold value of ≤ 1.95 , there is a sensitivity of 92.3% and a specificity of 50.0%.



squamous cell carcinoma of the head and neck is not definitively known, the finding likely relates to pathologic changes within the metastatic nodes. Reduced iodine content within metastatic lymph nodes compared with that within nonmetastatic lymph nodes has also been described in lung and colorectal carcinomas (11, 12). One possible explanation for the decreased iodine content is internal regions of necrosis that are not visibly perceptible. Another possible explanation is abnormal or reduced vascularity within metastatic nodes (10, 13, 14). One histopathological study of 65 patients with squamous cell carcinoma of the tongue who underwent nodal dissection found that the density of abnormal high endothelial venules was significantly higher in nodal metastases than in nonmetastatic lymph nodes (13). Furthermore, a histopathological evaluation of the lymph nodes in 16 patients with squamous cell carcinoma of the oral cavity or larynx/piriform fossa found that nonmetastatic lymph nodes had 1.4 times higher vessel density than metastatic lymph nodes (14). Future studies to evaluate the relationship between dual-energy–derived nodal iodine measurements and microscopic pathological analysis will be helpful to further investigate this relationship.

The spectral attenuation curve slope, another parameter used to evaluate lymph nodes in this study, was also significantly lower in metastatic lymph nodes than in control nodes. Furthermore, this significant difference persisted when the ratio of slopes for lymph node metastases to primary tumor was compared with the slopes of the control lymph nodes to primary tumor. These findings are intuitive given that the slope of the spectral attenuation curve in soft tissues depends greatly on the iodine content of the tissue. However, our findings are in contradiction to the findings of a prior study by Liang et al. who found that the slope of the spectral attenuation curve was higher in metastatic nodes than in control nodes (5). One possible explanation for this difference is that Liang et al. focused specifically on squamous cell carcinoma of the larynx and hypopharynx, whereas our study included only primary oropharyngeal carcinomas (5).

The current standard imaging techniques for the evaluation for nodal metastases in head and neck cancer include single-energy CT, MRI, US, and positron emission tomography (PET). In a meta-analysis of clinically NO head and neck cancer, which evaluated the results from 21 studies with histologically confirmed results, Liao et al. found no significant difference in sensitivity

between CT (52%, CI: 39%–65%), MRI (65%, CI: 34%–87%), US (66%, CI: 54%–77%), and PET (66%, CI: 47%–80%) (15). The specificity of CT (93%, CI: 87%–97%) was significantly better than the specificity of US (78%, CI: 71%–83%); however, there was no significant difference between the specificity of CT when compared with MRI (81%, CI: 64%–91%) or PET (87%, CI: 77%–93%) (15). Similarly, in Kyzas et al.'s meta-analysis, no significant difference was found in sensitivity or specificity for detecting nodal metastasis in squamous cell carcinoma of the head and neck between CT, MRI, 18F-FDG PET, and US–fine-needle aspiration (16). The ROC curves for this study show the potential additional sensitivity with reasonable specificity for nodal metastases that can be gained with DECT for quantification of nodal iodine content (sensitivity, 84%; specificity, 75%) and slope of the spectral attenuation curve (sensitivity, 92%; specificity 50%). Both values may prove to be useful adjuncts to contrast-enhanced CT examinations for the evaluation of patients with head and neck cancer.

Of the 8 patients included in this study, the HPV status was positive in 6 of the patients, negative in 1 patient, and unknown in the last patient. As the majority of our patients were HPV-positive, we did not feel that we could perform a meaningful analysis of the interaction between nodal disease (metastatic versus nonmetastatic) and HPV status in this study. Given the recent revision in the staging of squamous cell carcinomas in the head and neck to include HPV status, we believe that the impact of HPV on nodal iodine is an important area that should be investigated in future research.

One limitation of this study was the small sample size; however, the differences between iodine content and spectral attenuation curve slopes were still well within the realm of statistical significance. Although other studies have often included multiple primary malignancies of the head and neck resulting in an increased subject number, we feel that focusing specifically on primary oropharyngeal carcinoma and including only pathologically proven nodal disease strengthen this study despite its small size. Future work with larger patient populations would be helpful to further explore our findings.

Another limitation of this study was that the neuroradiologist performing the measurements was not blinded to the pathological status of the lymph nodes. Our goal in this study was to assess whether an identifiable difference in iodine content and

spectral slope was present between pathologically proven metastatic and nonmetastatic lymph nodes and if so to identify threshold values that can be used as markers for future studies. As such, we wanted the ROIs used in the study to be placed within nodes of known pathologic status and did not feel it was feasible for the neuroradiologist to accomplish this while blinded. With the threshold data established in this study, future studies can validate these thresholds for predicting metastatic involvement prospectively in lymph nodes by using readers who are blinded to the pathological status.

A final limitation of this study is the limitation of the DECT as a whole, which is that it is currently limited by the time required by

the radiologist to perform postprocessing. However, it is our belief that with the progression of machine learning, this limitation will likely be considerably reduced in the future.

CONCLUSIONS

Our study found significant differences in DECT-derived iodine content and spectral attenuation curve slopes between pathologically proven metastatic and nonmetastatic lymph nodes in patients with newly diagnosed oropharyngeal squamous cell carcinoma. Both of these measurements may be helpful tools to improve sensitivity and specificity of current imaging modalities in staging this group of patients.

Disclosures: No disclosures to report.

Conflict of Interest: The authors have no conflict of interest to declare.

REFERENCES

1. Siegel RL, Miller KD, Jemal A. Cancer statistics, 2017. *CA Cancer J Clin*. 2017; 67:7–30.
2. Sanderson RJ, Ironside JAD. Squamous cell carcinomas of the head and neck. *BMJ*. 2002;325:822–827.
3. Krestan C, Herneth AM, Formanek M, Czerny C. Modern imaging lymph node staging of the head and neck region. *Eur J Radiol*. 2006;58:360–366.
4. Johnson TRC. Dual-energy CT: general principles. *AJR Am J Roentgenol*. 2012; 199(5 Suppl.):3–8.
5. Liang H, Li A, Li Y, Cheng H, Zhao Q, Li J, Wang Q. A retrospective study of dual-energy CT for clinical detecting of metastatic cervical lymph nodes in laryngeal and hypopharyngeal squamous cell carcinoma. *Acta Otolaryngol*. 2015; 135:722–728.
6. Forghani R, Levental M, Gupta R, Lam S, Dadfar N, Curtin HD. Different spectral Hounsfield unit curve and high-energy virtual monochromatic image characteristics of squamous cell carcinoma compared with nonossified thyroid cartilage. *Am J Neuroradiol*. 2015;36:1194–1200.
7. Forghani R. Advanced dual-energy CT for head and neck cancer imaging. *Expert Rev Anticancer Ther*. 2015;13:1–13.
8. XLSTAT 2017: Data Analysis and Statistical Solution for Microsoft Excel. Addisonsoft, Paris, France (2017).
9. Puri SK, Fan CY, Hanna E. Significance of extracapsular lymph node metastases in patients with head and neck squamous cell carcinoma. *Curr Opin Otolaryngol Head Neck Surg*. 2003;11:119–123.
10. Tawfik AM, Razek AA, Kerl JM, Nour-Eldin NE, Bauer R, Vogl TJ. Comparison of dual-energy CT-derived iodine content and iodine overlay of normal, inflammatory and metastatic squamous cell carcinoma cervical lymph nodes. *Eur Radiol*. 2014;24:574–580.
11. Li X, Meng X, Ye Z. Iodine quantification to characterize primary lesions, metastatic and non-metastatic lymph nodes in lung cancers by dual energy computed tomography: an initial experience. *Eur J Radiol*. 2016;85:1219–1223.
12. Kato T, Uehara K, Ishigaki S, Nihashi T, Arimoto A, Nakamura H, Kamiya T, Oshiro T, Ebata T, Nagino M. Clinical significance of dual-energy CT-derived iodine quantification in the diagnosis of metastatic LN in colorectal cancer. *Eur J Surg Oncol*. 2015;41:1464–1470.
13. Lee SY, Chao-Nan Q, Seng OA, Peiyi C, Bernice WH, Swe MS, Chii WJ, Jacqueline HS, Chee SK. Changes in specialized blood vessels in lymph nodes and their role in cancer metastasis. *J Transl Med*. 2012;10:206.
14. Naresh KN, Nerurkar AY, Borges AM. Angiogenesis is redundant for tumour growth in lymph node metastases. *Histopathology*. 2001;38:466–470.
15. Liao LJ, Lo WC, Hsu WL, Wang CT, Lai MS. Detection of cervical lymph node metastasis in head and neck cancer patients with clinically NO neck-a meta-analysis comparing different imaging modalities. *BMC Cancer*. 2012;12:236.
16. Kyzas PA, Evangelou E, Denaxa-Kyza D, Ioannidis JPA. 18F-fluorodeoxyglucose positron emission tomography to evaluate cervical node metastases in patients with head and neck squamous cell carcinoma: A meta-analysis. *J Natl Cancer Inst*. 2008;100:712–720.